Journal of Magnetic Resonance 301 (2019) 67–72

Contents lists available at ScienceDirect

Journal of Magnetic Resonance

journal homepage: www.elsevier.com/locate/jmr

Saturation-recovery as a T_1-filter for T_2-T_2 exchange NMR

E.T. Montrazi *, T.J. Bonagamba

São Carlos Institute of Physics, University of São Paulo, PO Box 369, 13560-970 São Carlos, SP, Brazil

A R T I C L E   I N F O

Article history:
Received 11 January 2019
Revised 28 February 2019
Accepted 1 March 2019
Available online 2 March 2019

Keywords:
NMR
Exchange NMR
Saturation recovery
Porous materials

A B S T R A C T

The Inversion-Recovery (IR) technique has already been proposed to be used as a T_1-filter for $T_2 - T_2$ Exchange experiments. However, when the Exchange experiments are employed for studying samples that show T_1 distributions, where the pools are defined by broad relaxation time distributions, e.g. porous media, IR might be difficult to be used as a filter. This paper presents the difficulties found when using IR and proposes the use of Saturation-Recovery (SR) technique as an alternative to T_1-filter.

1. Introduction

The $T_2 - T_2$ Exchange experiment has been widely used to study molecular migration in porous media [1–16]. $T_2 - T_2$ Exchange experiment allows obtaining two-dimensional maps for a set of storage times (t_s), where the appearance of off-diagonal peaks is evidence of molecules migration across the pores. It corresponds to a three-dimensional pulse sequence, which demands a long experiment time. New sequences have been proposed to reduce the exchange experiment time. In 2009, Dortch et al. proposed a T_1-filter using the Inversion-Recovery (IR) before the $T_2 - T_2$ Exchange experiment [6,10]. Later on, in 2016, D'Eurydice et al. proposed to use the first CPMG in the $T_2 - T_2$ Exchange experiment as a T_2-filter [13,16]. Both filtered experiments reduce one dimension of the $T_2 - T_2$ Exchange experiment and, consequently, the experiment time. In these experiments, the only data obtained is the T_2 distribution measured during the second CPMG pulse sequence in the $T_2 - T_2$ Exchange experiment versus t_s, where the reappearance of filtered peaks are the evidence of exchange. Despite being a good method, there are some disadvantages when using IR as T_1-filter for systems presenting T_1 distributions where the pools are defined by broad relaxation time distributions. In the following section, the drawbacks of using IR as T_1-filter are discussed and Saturation-Recovery (SR) is proposed to circumvent them. To exemplify the application of the proposed method, it was used to study water molecules migration in the Portland Coombefield Whitbed Limestone sedimentary rock.

2. Theory

$T_2 - T_2$ Exchange or TREx (Transverse Relaxation Exchange) was proposed in 1993 by Lee et al. [1]. In 2009, Dortch et al. proposed to use IR before TREx to act as a T_1-filter and the sequence is shown in Fig. 1a. Combining the phase cycling, they demonstrated that the observed IR-TREx signal for each pool is given by [6].

$$\vec{M}_{IR-TREx}(t_{ir}, t_e, t_s, t_2) = 2\exp\left(\bar{L}_2 t_r\right)\exp\left(\bar{L}_1 t_s\right) \times \exp\left(\bar{L}_2 t_e\right)\left[1 - 2\exp\left(\bar{L}_1 t_{ir}\right)\right]\vec{M}_0, \quad (1)$$

where $\vec{M}_0$ is a vector containing the equilibrium magnetizations for each pool, $\bar{L}_1$ and $\bar{L}_2$ are matrices defined as sum of the relaxation and exchange matrices, t_{ir} is the inversion-recovery time, t_e is the CPMG excite time, t_s is the storage time, t_r is the CPMG readout time, and t_E the CPMG echo time.

The IR-TREx signal for given t_{ir} and t_s values corresponds to transverse relaxation decays, which can be inverted into a T_2 distribution using an inversion of a Fredholm integral algorithm (IFI) or using a multiple Gaussian-component fitting (MGF) [6,10]. Initially, the magnetizations of each pool are put in –Z direction, which return to +Z in a rate depending on their respective T_1 times, Fig. 1b. t_{ir} can be chosen in a way that one of the components is null in Z direction and, during the storage time, the nulled component will appear due to exchange with the non-nulled components, Fig. 1c (t_{ir}^1 and t_{ir}^2) [6,10]. For some t_{ir} values, the IR-TREx signal is a combination of decays with relative positive and negative amplitudes (Inverted Directions Region, in Fig. 1b and 1c (t_{ir}^3)), which

* Corresponding author.
E-mail address: elton.montrazi@usp.br (E.T. Montrazi).

https://doi.org/10.1016/j.jmr.2019.03.001
1090-7807/

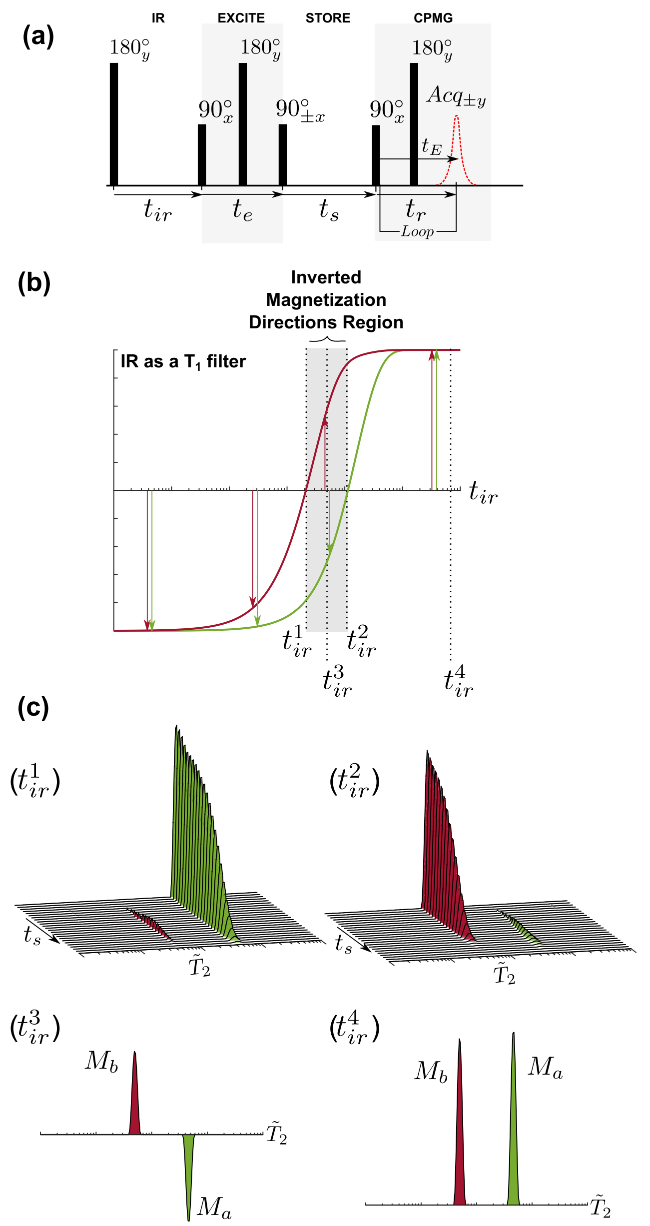

Fig. 1. (a) IR-TREx pulse sequence. The IR before the TREx is used as T_1-filter. (b) This figure illustrates the IR T_1-filter effects for a sample presenting two pools (A and B) with narrow T_1 distributions. The original proposal is that, for an appropriate t_{ir} value, the magnetization for one specific pool can be made null and, due to the exchange process during the storage time it can reappear and measured by CPMG. (c) $\tilde{T}_2$ distributions for some t_{ir} values. (t_{ir}^1) and (t_{ir}^2) illustrate the T_1-filters for pools A and B, respectively, and the signal evolution versus t_s. If t_{ir} is chosen zero or five times the longest T_1, for example (t_{ir}^4), the magnetizations have same direction. On the other hand, for some intermediate t_{ir} values as in (t_{ir}^3), the magnetizations can be in opposite directions, as exemplified in the Inverted Magnetization Region.

is a problem to the IFI algorithms that considers only positive magnetization values. To troubleshoot this, it is possible using MGF [6]. Now, considering that the exchanging pools have broadT_1 distributions, Fig. 2, there is an Inverted Magnetization Directions Region in the pool; this results in imperfect condition for zeroing all the magnetization of one pool. Trying nulling the magnetization using t_{ir} equal to the mean T_1 of the pool results in a magnetization distribution with positive and negative values, which is not predicted by IFI or MGF data processing.

All these IR drawbacks can be overcome with a very careful choice of t_{ir} or the use of Saturation-Recovery (SR) as T_1 filter.

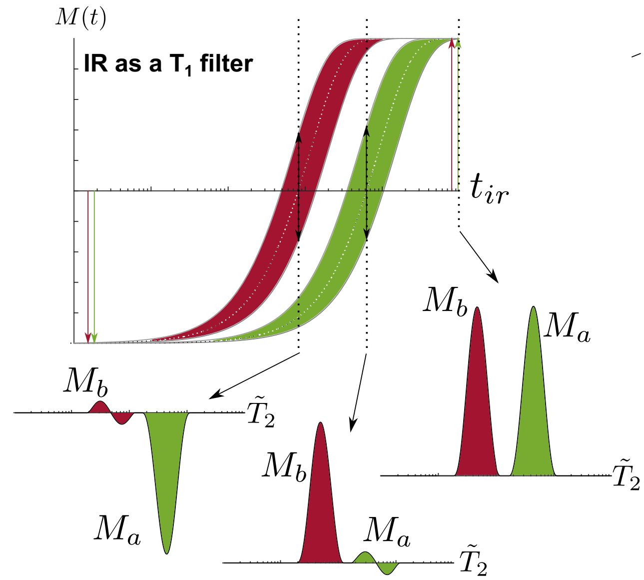

Fig. 2. Considering that the pools are composed by extended T_1 distribution, the condition of perfect annulation of the magnetization is not obtained. Trying nulling the pool using t_{ir} equal the mean T_1 of the pool, results in a signal of magnetization with positive and negative values as illustrated in the figure. There is an Inverted Magnetization Direction Region into the pool, and this type of signal is not predicted by IFI or MGF data processing.

When the SR is used, there are two advantages over IR: there are no Inverted Directions Regions and the recycle delay, normally five times T_1, can be very short. SR-TREx sequence is shown in Fig. 3. Fig. 3a describes the formal pulse sequence. However, it is not necessary to run the Saturation block (SR), as indicated in Fig. 3a, since at end of the CPMG block the spins are already saturated [17]. This is the way the experiments proposed are run, as indicated in Fig. 3b.

In the same way that Eq. (1) was obtained, it is easy to show that the observed SR-TREx signal for each pool is [6,10,13,16]

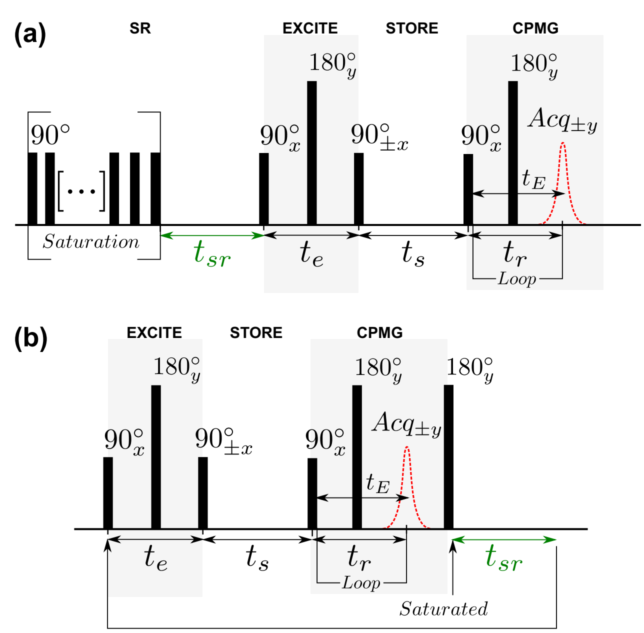

Fig. 3. (a) Formal SR-TREx pulse sequence. SR is used to act as T_1 filter for the TREx. (b) Used SR-TREx pulse sequence, where SR occurs during CPMG block.

$$\vec{M}_{SR-TREx}(t_{sr},t_e,t_s,t_2) = 2\exp\left(\bar{L}_2 t_r\right)\exp\left(\bar{L}_1 t_s\right) \times \exp\left(\bar{L}_2 t_e\right)\left[1-\exp\left(\bar{L}_1 t_{sr}\right)\right]\vec{M}_0, \quad (2)$$

where t_{sr} is the recovery time. Using the same approaches described by Dortch et al. and D'Eurydice et al., the peak amplitudes in the exchange curves is

$$\vec{P}_{SR-TREx}(t_{sr},t_e,t_s) = 2\left\{\bar{U}_{L_2}^{-1}\exp\left(\bar{L}_1 t_s\right)\exp\left(\bar{L}_2 t_e\right) \times \left[1-\exp\left(\bar{L}_1 t_{sr}\right)\right]\vec{M}_0\right\}^{\circ}\left(\bar{1}_{1\times N}U_{L_2}\right)^{T}, \quad (3)$$

where $\bar{1}_{1\times N}$ is a vector of ones, $\circ$ represents the element-wise matrix multiplication operation, U_{L_2} is a matrix whose columns are the corresponding eigenvectors obtained by the $\exp\left(\bar{L}_2 t_r\right)$ expansion, and the superscript T represents the matrix transpose operation [6,10,13,16].

In the context of the exchange phenomena, it is important to remember that the relaxation time measured by the traditional experiments like IR, SR and CPMG are apparent relaxation times [6,10,13,16],

$$\tilde{T}_{1,2} = \frac{1}{\lambda_{L_{1,2}}} \quad (4)$$

where $\lambda_{L_{1,2}}$ are the eigenvalues obtained by the $\exp\left(\bar{L}_{1,2} t\right)$ expansion.

3. Materials and methods

Portland Coombefield Whitbed Limestone (CWL) sedimentary rock with diameter and height equal to 38.1 mm was used to demonstrate the applicability of the proposed method.

Firstly, porosity and permeability were both measured by dry helium gas intrusion, resulting in the following values: $(18.9 \pm 0.1)\%$ and (47.3 ± 0.1) mD, respectively. Afterwards, the core was divided into two pieces with diameter equal to 10 mm and height to 7 mm for NMR and mercury injection capillary pressure (MICP) measurements, and a thin section of $15 \times 30 \times 2$ mm for optic microscopic analysis.

CWL is an oolitic limestone from the Portlandian formation. The rock is formed from micrite ooids with a small quantity of micrite occurring as matrix that can be observed in the thin-section, Fig. 4 [18,19].

From thin-section analysis, it can be concluded that there are microporosities and macroporosities associated with micritc ooliths and intergranular macropores, respectively. Additional porosity details were obtained from MICP, Fig. 5, where it can be observed micropore- and macropore-throat distributions in the ranges of 10^{-2} to 10^{0} μm (peak B) and 10^{1} to 10^{2} μm (peak A), respectively [18].

NMR experiments were performed in water saturated CWL, at room temperature, using a TECMAG Redstone spectrometer, associated with an Oxford 2 T superconducting magnet and operating at ^{1}H Lamor frequency of 85 MHz. A CPMG measurement was performed under 0.047 T (2 MHz) to ensure that induced internal gradients would not influence the T_2 distributions at 2 T (85 MHz).

Firstly, CPMG was used to obtain and assign the T_2 peaks observed to the pores identified by MICP. Afterwards, the SR-TREx experiments were performed using an array with 16 logarithmically spaced t_{sr} recovery times, ranging from 5 ms to 15 s, in order to show the SR T_1-filter behavior. t_E and t_s were fixed to 200 μs and 1 ms, respectively, CPMG encoding was set to 10 echoes, and 30,000 echoes were acquired. The filter curves and

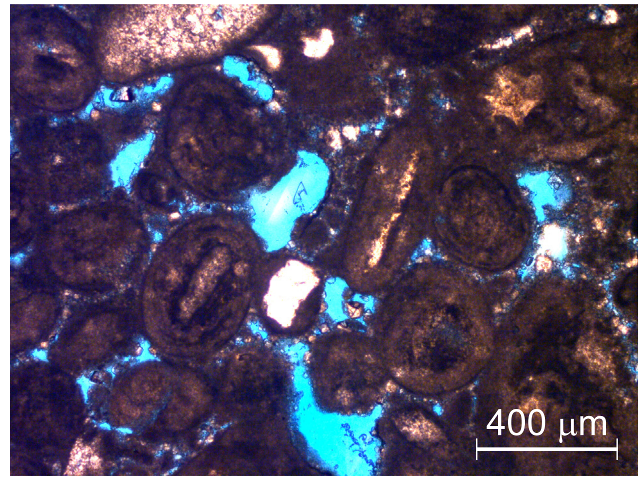

Fig. 4. Optical micrograph of the CWL thin-section. The regions in blue are the pores that were filled with blue epoxy used on the manufacturing of the thin-section. The dark and white structures are micritc ooliths. It is observed porosity associated with intergranular macropores and intercrystalline microporosity associated with micritc ooliths. (For interpretation of the references to colour in this figure legend, the reader is referred to the web version of this article.)

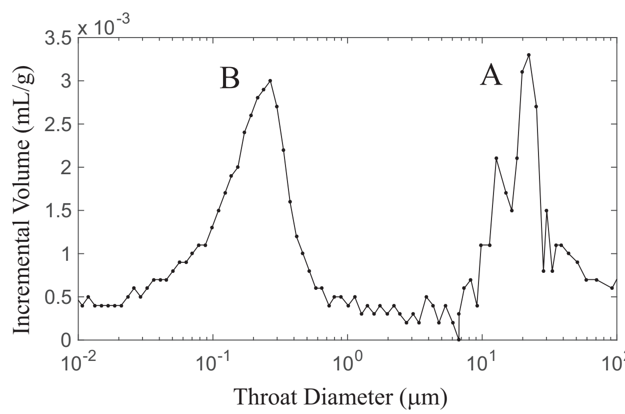

Fig. 5. Mercury injection capillary pressure (MICP) from CWL. It is possible to classify two pore-throat size distributions. Peak A refers to macropores and peak B to micropores.

$\tilde{T}_2$ distributions versus t_{sr}, were obtained by using 1D-IFI [20].

Choosing some t_{sr} values from the filter curves, the SR-TREx experiment was performed using an array with 32 logarithmically spaced storage times, t_s ranging from 1 ms to 10 s. The acquisition method described by Montrazi et al. [16] was applied to acquire simultaneously the SR-TREx curves and the $\tilde{T}_1 - \tilde{T}_2$ map, the latter obtained by using 2D-IFI [21] and $\tilde{T}_2$ distributions versus t_s by 1D-IFI [20].

The exchange curves and exchanging pool peak amplitudes as a function of t_s were obtained by log-normal fittings approach, and the exchange rates $k_{ij}'s$ as well as the real times $T_1's$ and $T_2's$ were estimated using Eq. (3), both methods described by Montrazi et al. [16].

In order to compare the parameters obtained by the SR-TREx method, $k_{ij}'s$, $T_1's$ and $T_2's$, the T_2-Filtered $T_2 - T_2$ Exchange experiments (T_2F-TREx) were performed using the same t_E and t_s values used to run SR-TREx experiments. For the T_2F-TREx experiments, two CPMG T_2-filters times denoted by t_f were used, 40 and 160 ms, which correspond to 200 and 800 echoes, respectively. t_f is defined by number of π pulses times t_E [13].

4. Results and discussions

Fig. 6 shows the $\tilde{T}_2$ distributions at 2 and 85 MHz, CPMG and SR-TREx for the series of t_{sr}, respectively. The $\tilde{T}_2$ distribution obtained by SR-TREx with t_{sr} = 15,000 ms corresponds to a CPMG signal at 85 MHz. As $\tilde{T}_2$ distributions obtained in low and high field are very similar, one can suppose that induced internal gradients are not important for the next discussions.

For all $\tilde{T}_2$ distributions, two types of pools were assigned, which can be represented by two log-normal distributions, Fig. 6. Considering that the CWL is constituted almost in total by micrite, one can suppose that all the pores present practically the same surface relaxativity. Consequently, T_2 can be directly associated with the pore size: shorter T_2 times with microporosity (pool B) and longer T_2 times with macroporosity (pool A).

The SR T_1-filter efficiency analysis is shown in Fig. 6. Varying t_{sr} in the SR method, the pool B, with shorter T_1 times, recovers faster than pool A, with longer T_1 times. Then, for shorter t_{sr} is observed that the pool B with presents a lot of magnetization relatively to pool A. This fact was used to evidence the exchange from B to A that was observed next in the exchange curves.

Three t_{sr} values were chosen from the filters curves to perform the SR-TREX: 15, 358 and 15,000 ms (see Fig. 6). To compare the results obtained from the SR-TREx method, the T_2F-TREx experiment was performed for t_f equal 200 and 800 echoes.

Both SR-TREx and T_2F-TREx signals were measured by the Simultaneous Acquisition method in order to obtain the $\tilde{T}_1 - \tilde{T}_2$ correlation map, Fig. 7 [16]. The macro and microporosity, peaks A and B respectively, were classified as done to the $\tilde{T}_2$ distribution.

In the $\tilde{T}_2$ distributions projections of the $\tilde{T}_1 - \tilde{T}_2$ correlation map were fitted the log-normals, which are presented in yellow

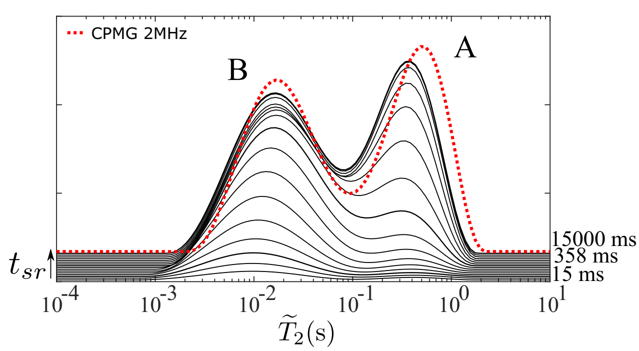

Fig. 6. Apparent transverse relaxation times distributions of saturated CWL sample obtained with SR-TREx for different recovery times. For t_{sr} = 15000 ms, the signal is similar to a CPMG experiment, and this $\tilde{T}_2$ distribution can be associated with MCIP results. It is important to observe that the pools with shorter T_1 times recover faster than longer T_1 times. The thick lines represent the conditions for the chosen filters. For comparison, the $\tilde{T}_2$ distribution obtained at 2 MHz is also presented.

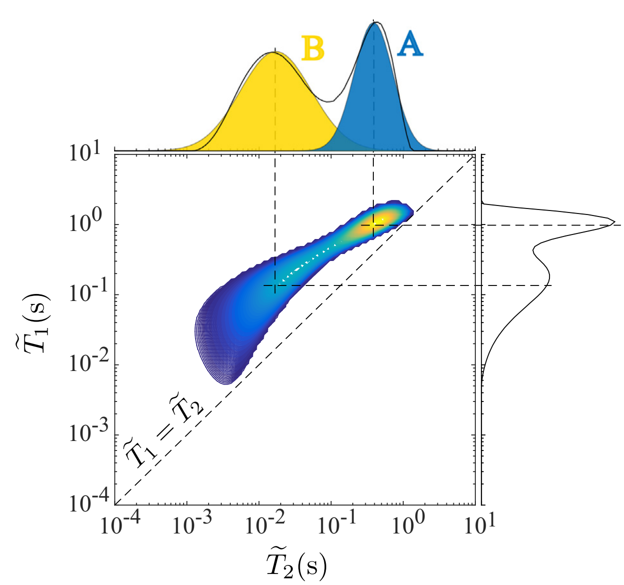

Fig. 7. $\tilde{T}_1 - \tilde{T}_2$ correlation map of water saturated CWL obtained via Simultaneous Acquisition [16]. The peak with the highest relaxations times is related to macroporosity (peak A) and the peak with the smallest values of $\tilde{T}_1$ and $\tilde{T}_2$ is related to microporosity (peak B).

Table 1
Apparent equilibrium magnetizations and apparent longitudinal and transverse relaxation times determined through the log-normals fitting.

$\tilde{M}_0^A$ (%)	$\langle\tilde{T}_2\rangle^A$ (s)	$\langle\tilde{T}_1\rangle^A$ (s)
41.4	0.38	0.98
$\tilde{M}_0^B$(%)	$\langle\tilde{T}_2\rangle^B$ (s)	$\langle\tilde{T}_1\rangle^B$ (s)
58.6	0.017	0.13

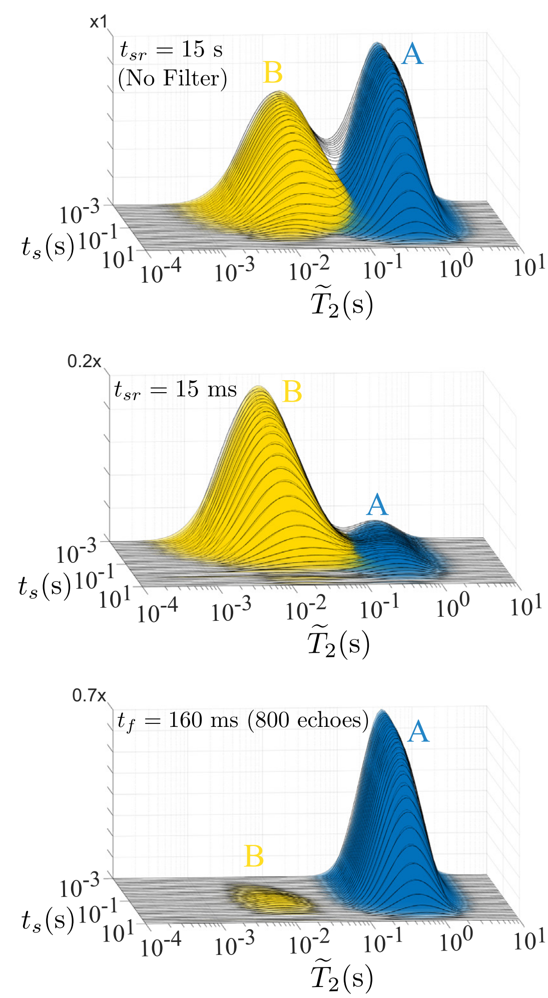

Fig. 8. $\tilde{T}_2$ distributions versus t_s. For t_{sr} equal to 15 ms, it is noted that the pool B has a lot of magnetization relatively to pool A. Thus, the exchange of pool B to pool A is evidenced, the peak A amplitude increase and decrease in function of t_s. For t_{sr} = 15 s, there are no filter effects and peak amplitudes only decay.

and blue in Fig. 7. The mean apparent transverse times, $\langle\widetilde{T}_2\rangle$, and the apparent equilibrium magnetization, $\widetilde{M}_0$, calculated through the fitting process are summarized in Table 1. The mean apparent longitudinal times, $\langle\widetilde{T}_1\rangle$, were adjusted by the maximum $\widetilde{T}_1$ correspondent to the $\langle\widetilde{T}_2\rangle$ obtained values.

Fig. 8 shows the $\widetilde{T}_2$ distributions as a function of t_s for t_{sr} = 15 ms, t_f = 160 ms (800 echoes) and t_{sr} = 15 s (No Filter) that correspond a condition without filter to SR-TREx and T_2F-TREx

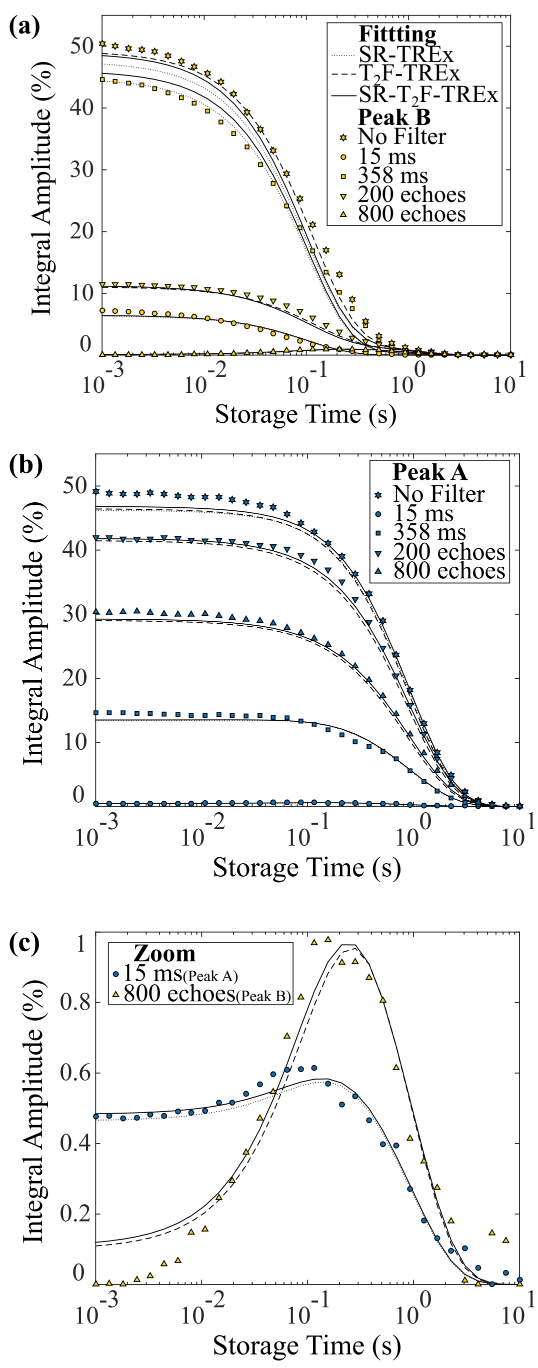

Fig. 9. (a) and (b) Exchange curves: integral amplitude of each peak versus t_s for No Filter, T_1-filter (15 and 358 ms), and T_2-filter (200 and 800 echoes). (c) Zoom from the exchange curves of peak A, for t_{ir} =15 ms, and peak B, for t_s =800 echoes. For these filters, it can be observed that the amplitudes of filtered peaks first increases and then decrease, as already discussed above in Fig. 8.

Table 2
Apparent and real relaxation times, real equilibrium magnetizations, and characteristic exchange times ($k_{ij} = 1/\tau_{ij}$) obtained by the SR-TREx method, T_2F-TREx method and both simultaneously, SR-T_2F-TREx.

	SR-TREx	T_2F-TREx	SR-T_2F-TREx
$M_0^A(\%)$	0.46	0.45	0.46
$M_0^B(\%)$	0.54	0.55	0.54
$\langle T_1^A\rangle$(s)	1.81	1.54	1.91
$\langle T_1^B\rangle$(s)	0.10	0.12	0.11
$\langle T_2^A\rangle$(s)	0.48	0.40	0.42
$\langle T_2^B\rangle$(s)	0.017	0.026	0.026
τ_{AB}(s)	1.8	1.9	1.7
τ_{BA}(s)	2.1	2.4	2.0
$\langle\widetilde{T}_1^A\rangle$(s)	0.92	0.89	0.93
$\langle\widetilde{T}_1^B\rangle$(s)	0.10	0.11	0.10
$\langle\widetilde{T}_2^A\rangle$(s)	*0.38**	0.34	0.34
$\langle\widetilde{T}_2^B\rangle$(s)	*0.017**	0.025	0.026

* Fixed $\widetilde{T}_2$'s values obtained in the $\widetilde{T}_1 - \widetilde{T}_2$ map, Table 1.

experiments. For the case where filters are not applied, the magnetization of each pool decays according to the apparent longitudinal time, $\widetilde{T}_1$. For t_{sr} = 15 ms, it is observed that the magnetization of pool B is bigger than that of pool A. During the increase storage time, the amplitude of the pool A, which was filtered, first increases, due to the exchange process, and subsequently decreases, due to T_1 relaxation. This t_{sr} dependence is clearly seen in the exchange curves presented below. For t_f = 160 ms (800 echoes) the pool B is totally filtered and, because of that, it is easy to observe the recuperation of the filtered pool during the storage time.

The log-normals were fitted to the $\widetilde{T}_2$ distributions, curves yellow and blue in Fig. 8, and, thereby, the exchange curves were obtained, Fig. 9. The exchange process in SR-TREx is evidenced by the amplitude recuperation of the peak A for 15 ms of t_{sr} and the recuperation of the peak B for T_2F-TREx with t_f of 800 echoes (Fig. 9c).

The filter of T_2F-TREx is a function of T_2 while the storage time is a function of T_1. In this case, the exchange curves can be fitted simultaneously without restriction. However, for the SR-TREx or IR-TREx experiments, the filter and the storage time are both functions of T_1. Therefore, there is weak information of T_2 in the exchange curves and the T_2 values can diverge. Because of this, it is necessary combine the SR-TREx or IR-TREx results with, e.g., a CPMG result as done by Dortch et al. [10] Here, to fitting the SR-TREx results, $\widetilde{T}_2$'s values were forced to be equal to obtained in the $\widetilde{T}_2$ distribution, Table 1.

The fitting on the exchange curves, Fig. 9, was done for the SR-TREx results, the T_2F-TREx results and both simultaneously, SR-T_2F-TREx, in order to compare the methods. The T_2F-TREx exchange curves were fitted using the equations and method described by Montrazi et al. [16]. For the SR-TREx results, Eq. (3) was used to fit the exchange curves with $\widetilde{T}_2$'s values from Table 1. The adjusted parameters obtained are shown in Table 2.

The parameters obtained through the methods used are consistent among them. Also, the real equilibrium magnetizations and apparent relaxation times are in agreement with values presented in Table 1.

5. Conclusion

When the pools present wide T_1 distributions, as usual, more attention is needed in the use of the IR as a T_1-filter for $T_2 - T_2$

Exchange, since it introduces some important drawbacks, as discussed along the paper. Differently, the proposed SR filter is free of those problems, which can be used without very careful adjustments. It is important to have a good T_1-filter, such as SR, because it can be used in combination with the T_2-filter to enrich the information obtained by the Exchange experiments, as shown here.

Acknowledgements

This study was financed in part by the Coordenação de Aperfeiçoamento de Pessoal de Nível Superior - Brasil (CAPES) – Finance Code 001, Conselho Nacional de Desenvolvimento Científico e Tecnológico – Brasil (CNPq), Fundação de Amparo à Pesquisa do Estado de São Paulo – Brasil (FAPESP) (Project: 2009/54880-6), Agência Nacional do Petróleo – Petrobras – Brasil (ANP) (Projects: 2012/00380-5 and 2015/00416-8), and Universidade de São Paulo (USP). Authors acknowledge André Souza (Schlumberger) for the Coombefield Whitbed Limestone sample, porosity and permeability results, as well as the description of the thin-section.

References

[1] J.H. Lee, C. Labadie, C.S. Springer, G.S. Harbison, Two-dimensional inverse Laplace transform NMR: altered relaxation times allow detection of exchange correlation, J. Am. Chem. Soc. 115 (1993) 7761–7764.
[2] P. McDonald, J.-P. Korb, J. Mitchell, L. Monteilhet, Surface relaxation and chemical exchange in hydrating cement pastes: a two-dimensional NMR relaxation study, Phys. Rev. E 72 (2005), 1–9.
[3] L. Monteilhet, J.-P. Korb, J. Mitchell, P. McDonald, Observation of exchange of micropore water in cement pastes by two-dimensional T_2–T_2 nuclear magnetic resonance relaxometry, Phys. Rev. E 74 (2006) 1–9.
[4] K. Washburn, P. Callaghan, Tracking pore to pore exchange using relaxation exchange spectroscopy, Phys. Rev. Lett. 97 (2006), 25–28.
[5] J. Mitchell, J.D. Griffith, J.H.P. Collins, A.J. Sederman, L.F. Gladden, M.L. Johns, Validation of NMR relaxation exchange time measurements in porous media, J. Chem. Phys. 127 (2007) 234701.
[6] R.R. Dortch, R. Horch, M.D. Does, Development, simulation, and validation of NMR relaxation-based exchange measurements, J. Chem. Phys. 131 (2009) 164502.
[7] M. Fleury, J. Soualem, Quantitative analysis of diffusional pore coupling from T2-store-T2 NMR experiments, J. Colloid Interface Sci. 336 (2009) 250–259.
[8] M. Van Landeghem, A. Haber, J.B.D. Lacaillerie, B. Blümich, Concepts in Magnetic Resonance Part A, 36A, 153-169, 2010. Analysis of Multisite 2D Relaxation Exchange NMR.
[9] J. Mitchell, T.C. Chandrasekera, M.L. Johns, L.F. Gladden, E.J. Fordham, Nuclear magnetic resonance relaxation and diffusion in the presence of internal gradients – the effect of magnetic field strength, Phys. Rev. E 81 (2010) 1–19.
[10] R.D. Dortch, K.D. Harkins, M.R. Juttukonda, J.C. Gore, M.D. Does, Characterizing inter-compartmental water exchange in myelinated tissue using relaxation exchange spectroscopy, Magnet. Reson. Med. 70 (2013) 1450–1459.
[11] L.M. Schwartz, D.L. Johnson, J. Mitchell, T.C. Chandrasekera, E.J. Fordham, Modeling two-dimensional magnetic resonance measurements in coupled pore systems, Phys. Rev. E 88 (2013) 032813.
[12] D.L. Johnson, L.M. Schwartz, Analytic theory of two-dimensional NMR in systems with coupled macro- and micropores, Phys. Rev. E 90 (2014) 032407.
[13] M.N. D'Eurydice, E.T. Montrazi, C.A. Fortulan, T.J. Bonagamba, T2-filtered T2–T2 exchange NMR, J. Chem. Phys. 145 (2016), 154202.
[14] R. Song, Y.-Q. Song, M. Vembusubramanian, J.L. Paulsen, The robust identification of exchange from T_2–T_2 time-domain features, J. Magn. Reson. 265 (2016) 164–171.
[15] R. Bai, D. Benjamini, J. Cheng, P.J. Basser, Fast, accurate 2D-MR relaxation exchange spectroscopy (REXSY) Beyond compressed sensing, J. Chem. Phys. 145 (2016) 154202.
[16] E.T. Montrazi, E. Lucas-Oliveira, A.G. Araujo-Ferreira, M. Barsi-Andreeta, T.J. Bonagamba, Simultaneous acquisition for T2–T2 exchange and T1–T2 correlation, J. Magnet. Reson. 289 (2018) 63–71.
[17] A. Sezginer, R.L. Kleinberg, M. Fukuhara, L.L. Latour, Very rapid simultaneous measurement of nuclear magnetic resonance spin-lattice relaxation time and spin-spin relaxation time, J. Magn. Reson. 92 (1991) 504–527.
[18] J.P. Ingham, Predicting the frost resistance of building stone, Q. J. Eng. Geol. Hydrogeol. 38 (2005) 387–399.
[19] http://projects.bre.co.uk/ConDiv/stonelist/portcoomb.html.
[20] G.C. Borgia, R.J.S. Brown, P. Fantazzini, Uniform-penalty inversion of multiexponential decay data, J. Magnet. Resonance 132 (1998) 65–77.
[21] L. Venkataramanan, Y.-Q. Song, M.D. Hürlimann, Quantitative characterization of food products by two-dimensional D-T_2 and T_1–T_2 distribution functions in a static gradient, J. Colloid Interface Sci. 297 (2006) 303–311.